Generation of Suprathermal Electrons during Magnetic Reconnection at the Sawtooth Crash and Disruption Instability in the T-10 Tokamak

P. V. Savrukhin

Russian Research Center "Kurchatov Institute," 123182, Moscow, Russia

(Received 31 July 2000)

Evidence for excitation of suprathermal electrons ($E_\gamma \sim 20-100$ keV) during magnetic reconnection in the T-10 tokamak is presented through analysis of the x-ray measurements with enhanced spatial and time resolution. A toroidally viewing x-ray imaging system and a fast hard x-ray detector placed inside the tokamak vessel allow identification of bursts of the nonthermal x-ray radiation around X points of the $m = 1$ and $m = 2$ magnetic islands during the sawtooth crash and prior to the energy quench at the density limit disruption.

DOI: 10.1103/PhysRevLett.86.3036 PACS numbers: 52.55.Fa, 52.35.Py, 52.70.La

Magnetic reconnection involves breaking and topological rearrangement of magnetic field lines and induces relaxation processes in a wide range of laboratory plasmas [1–3] and astrophysics phenomena [4,5]. The reconnection process can occur in a current sheet layer formed when two volumes of highly conducting plasma with opposite magnetic fields are pushed against each other. The dynamics of the sheet current and annihilation of the perturbed magnetic fluxes during the reconnection are generally determined by nonideal effects in Ohm's law such as collisional resistive diffusion, electron viscosity and inertia, as well as magnetic turbulence (see [2]). However, in weakly collisional plasma, dissipation of the magnetic energy can be additionally influenced by high-energy electrons accelerated during the reconnection [1,2]. Acceleration of electrons by the electric field is balanced at the first instant by the drug caused by Coulomb collisions. The collision frequency decreases with increasing electron velocity. This implies that above a certain critical velocity electrons are continuously accelerated ("runaway" [6]) until they became a subject of additional loss mechanisms connected with kinetic instability or synchrotron radiation [7]. Observation of nonthermal electrons during reconnection is the primary task of the present experiments.

The reconnection process has attracted particular attention in experiments in tokamaks during analysis of plasma disruptions and internal relaxations (sawteeth) [8,9]. Instability in this case is characterized by the growth of helical plasma perturbations (MHD modes) with low toroidal and poloidal mode numbers (e.g., $n = 1-2$, $m = 1-3$, accordingly) resonant on magnetic surfaces with rational values of the safety factor q (here, $q = d\Psi_t/d\Psi_p$, Ψ_t, Ψ_p are toroidal and poloidal magnetic fluxes, accordingly). In tokamak plasma with finite magnetic shear [$s = (r/q)dq/dr > 0$] growth of the m/n mode leads to squeezing of the field lines around resonant magnetic surfaces with $q = m/n$ and subsequent abrupt redistribution of magnetic and thermal energy which is described by the reconnection theory [1].

Plasma disruptions in tokamaks are often accompanied by bursts of nonthermal x-ray and electron-cyclotron emission (see review [9]). Detailed experiments made recently in JET [10], JT-60U [11], and TEXTOR [12] have indicated such bursts can be connected with the interaction of MHD modes with the population of high-energy electrons. However, most of the previous experimental studies considered the postdisruption plasma [10], while analysis of nonthermal electrons in flight during the reconnection has not been completed so far. Moreover, analysis of runaway electrons in laboratory experiments is additionally complicated by localization of nonthermal radiation in the narrow forward cone along the particle trajectory, which limits application of standard x-ray diagnostics with line of sight orthogonal to the plasma column. Measurements of x-ray radiation in the direction tangential to the magnetic field lines with enhanced time and spatial resolution in present experiments in T-10 clarify the problem by explicitly showing the localization and time evolution of nonthermal x-ray emission during the reconnection process.

The experiment was performed at the T-10 tokamak in the Kurchatov Institute (major and minor radii, $R_0 = 1.5$ m, $a = 0.3$ m, accordingly). Plasma perturbations are analyzed with the use of the toroidally viewing x-ray imaging system (TX array) [13] (1), standard x-ray tomographic arrays [14] XRA, XRB, XRC (2)–(4), and x-ray gas detector (5) (see Fig. 1). The TX array consists of a 2 by 2 set of silicon diodes placed inside the tokamak vacuum vessel at the low-field side of the torus (energy range of the measured x rays $E_\gamma \geq 2.5$ keV). Angular orientation of the TX array can be changed between the tokamak pulses, which allows measurements of x-ray radiation from the bulk part of the plasma ($r/a \geq 0.25$) with radial resolution $\delta \sim 7$ mm. Additional silicon diode HXR (6) is placed inside the TX array for measurements of the suprathermal x-ray emission ($E_\gamma \geq 45$ keV). Hard x-ray emission ($E_\gamma \sim 0.5-3.0$ MeV) is measured using the standard NaI(Tl) detector (7). A germanium detector (8) is used for identification of the x-ray spectra from the pulse height

 0031-9007/01/86(14)/3036(4)$15.00

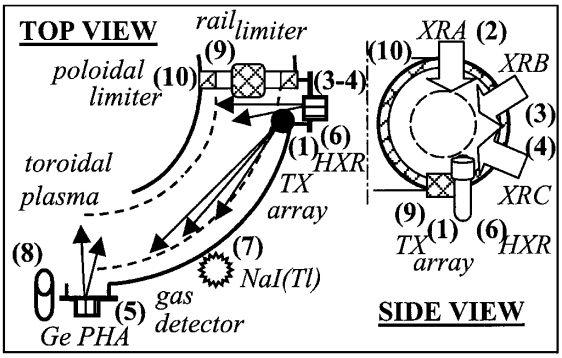

FIG. 1. Experimental setup shown schematically. The x-ray perturbations are measured with the tangentially viewing (TX) array (1) [13], imaging system (2)–(4) [14], gas detector (5), silicon diode (6), NaI(Tl) monitor (7), and Ge PHA spectrometer (8).

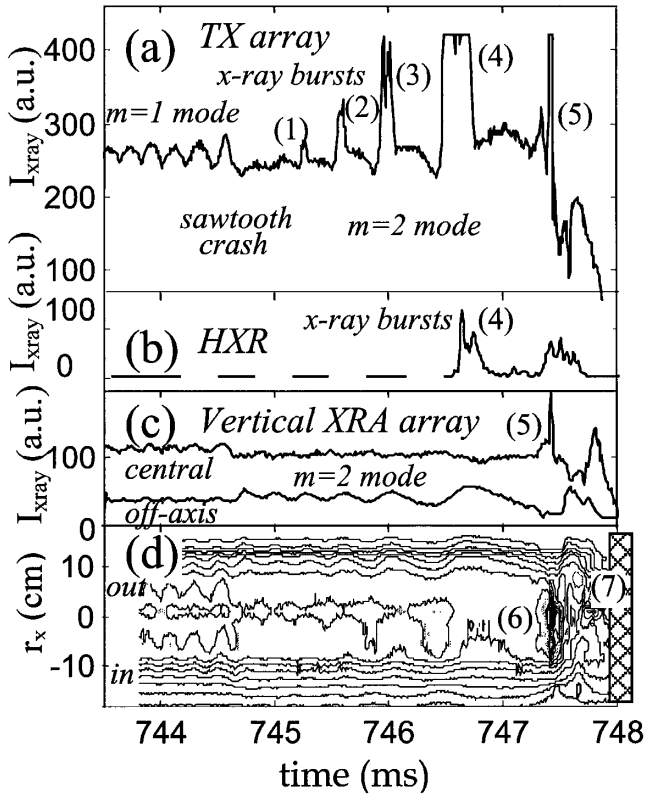

FIG. 2. Time evolution of x-ray intensity and x-ray contour plot measured with the tangential array (a), in-vessel HXR detector (b), and vertical XRA array (c),(d) prior the density limit disruption. Energy quench ($t \sim 747.5$ ms) is preceded by nonthermal x-ray bursts (1)–(6) superimposed with the $m = 2$ mode. Projection of the rail limiter at the counter plot is shown schematically by rectangle (7).

analysis (PHA). Plasma in T-10 is restrained by a movable rail limiter (9) and guard poloidal limiter (10).

Plasma perturbations in T-10 are studied at the radiative density limit disruption in Ohmically heated plasma (plasma current, $I_p = 0.2–0.3$ MA, toroidal magnetic field, $B_t = 2–2.4$ T, electron density, $n_e = 3–4.5 \times 10^{19}$ m^{-3}). Energy quench in such conditions [14] is preceded by coupling of the $m = 1$ and $m = 2$ ($n = 1$) modes with subsequent slowing down of the modes rotation. Measurements of x-ray intensity in the toroidal direction using TX array indicate that just prior to disruption, the $m = 2$ mode becomes superimposed with periodic bursts of x-ray radiation [see marks (1)–(5) in Figs. 2a and 2b]. The x-ray bursts are not observed with conventional x-ray arrays and gas counter with orthogonal field of view (see Fig. 2c). This indicates preferred emission in the forward cone around the equatorial midplane, which is typical for nonthermal electrons [10]. Analysis of the TX and conventional x-ray data indicates that the bursts are localized around X points of the $m = 2$ magnetic islands. Energy quench at the density limit is initiated during the consecutive x-ray burst [see mark (5) in Fig. 2] at the moment when X point of the $m = 2$ magnetic island is placed in front of the rail limiter. In contrast with bursts (1)–(4), the x-ray spike (5) is observed also with conventional x-ray detectors looking along central vertical chords, which can indicate interaction of electron beams with the narrow spot at the limiter [see mark (6) in Fig. 2d]. Analysis of localization of the bright spot (6) and time duration of the bursts shows that nonthermal electrons are placed within 25% of the $m = 2$ island wavelength. Such narrow localization of radiation bursts differs from conventional spikes of hard x-ray emission after the energy quench measured with all x-ray arrays and NaI(Tl) monitor when avalanches of the runaway electrons fill the plasma volume and hit the limiters.

Experiments in T-10 indicate that internal relaxations (sawtooth crashes) are also preceded by spikes of nonthermal radiation [see mark (1) in Fig. 3a]. The spikes at sawtooth crashes are generally observed during the last cycle of rotation of the $m = 1$ mode. Amplitude of the x-ray spike is maximal around the sawtooth inversion surface ($q = 1$ surface), $r = r_s$ (Fig. 3b). In contrast with the density limit disruption (see Fig. 2), spikes during sawtooth crashes are also observed with conventional x-ray arrays. Analysis of x-ray intensity in this case indicates that during the crash, the spike moves in a "poloidal" direction accordingly with rotation of the $m = 1$ mode (see $t1–t5$ in Fig. 3c). Analysis of local x-ray emissivity determined from the experimental data using Cormack algorithms (see [14]) indicates that the spike is superimposed with a maximum perturbation due to the $m = 1, n = 1$ mode, which can be associated with the X point of the magnetic island (Fig. 3d). In subsequent sawtooth crashes nonthermal spikes can be initiated at either the low or high field side of the torus, which seems to exclude the possible ballooning origin of the perturbations (see [15,16]). Just after the sawtooth crash x-ray spikes are observed outside the $q = 1$ surface at the top of the heat pulse propagating through the plasma to larger radii ($r/a \leq 0.7$) on a time scale of the order of $\delta t \sim 0.1$ ms (see Fig. 4e).

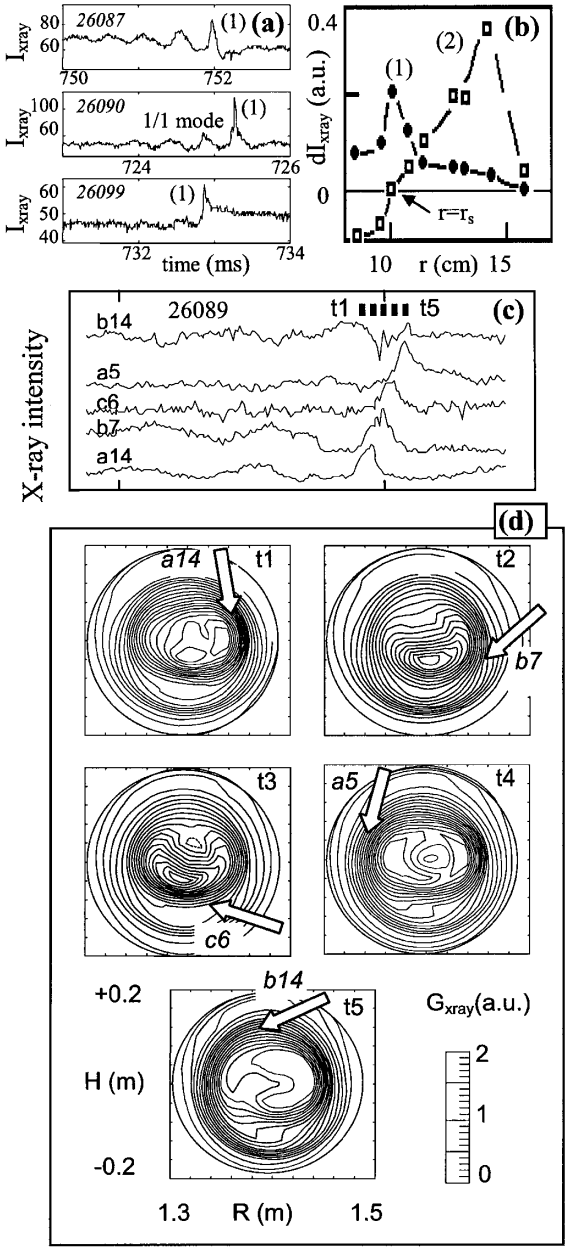

FIG. 3. Time evolution of the x-ray intensity (a) and radial profiles of the x-ray perturbations (b) measured with the TX array during the nonthermal spikes (1) and sawtooth crashes (2) in subsequent tokamak pulses [(26087) $r < r_s$, (26090) $r \sim r_s$, (26099) $r > r_s$]. (c) Time evolution of the x-ray intensity measured along chords tangential to the $q = 1$ surface using conventional x-ray arrays and (d) tomographic images of the x-ray emissivity, G_{xray} ($t1 = 742.968$ ms, $t2 = 743.008$ ms, $t3 = 743.056$ ms, $t4 = 743.080$ ms, and $t5 = 743.104$ ms). The x-ray spike is observed consecutively along chords with various pitch angle starting from the equatorial midplane: $\theta \approx 0°$ ($a14$), $\theta \approx -60°$ ($b7$), $\theta \approx -120°$ ($c6$), $\theta \approx -180°$ ($a5$), $\theta \approx -240°$ ($b14$).

Analysis of angular and energy distribution of the x-ray radiation measured with various x-ray arrays in the T-10 experiments has indicated that the energy of the runaway electrons in flight is of the order of 20–100 keV. Mea-

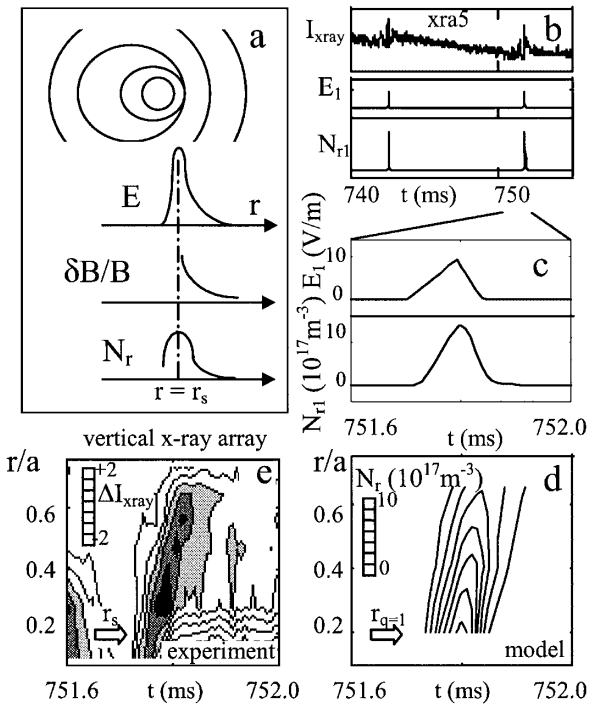

FIG. 4. (a) Schematic view of magnetic flux surfaces ($m = 1$ mode) and radial profiles of the longitudinal electric field E, magnetic field perturbations $\delta B/B$, and runaway electron density N_r used in the simulations of the sawtooth relaxation. Frames (b) and (c) illustrate calculated time evolution of the runaway beam density (N_{r1}) induced by electric field (E_1) around the $q = 1$ surface in subsequent sawtooth crashes specified from the experiments (see $xra5$-$t = 742.6$ ms and $t = 751.8$ ms). Frames (e) and (d) represent, accordingly, the contour plot of x-ray perturbations measured during the sawtooth crash and calculated electron density (N_r) at outer radii. Radial localization of the x-ray bursts [see dark area in frame (e)] coincides with outward displacement of the runaway beam.

surements of the x-ray spectrum using Ge PHA spectrometer indicate appearance of the nonthermal electrons in the specified energy range during density limit disruption. However, poor time resolution of the PHA analysis ($\delta t \sim 0.1$ s) did not allow one to determine unambiguously temporal modifications of the spectrum during the disruption.

Production of runaway electrons during disruption has been the subject of a number of theoretical investigations [6,7,17]. In a simplified way, time evolution of the density of runaway electrons (N_r) generated with the application of electric field (E) in thermal plasma with density n_e can be described by the equation

$$\partial N_r/\partial t + \nabla \cdot (\mathbf{v}_r N_r) = n_e/\tau_{dr} + N_r/\tau_{av} - N_r/\tau_{\mathrm{loss}},$$

where $|\mathbf{v}_r| \sim 0.5c$ is the runaway electron mean velocity, $1/\tau_{dr}$ and $1/\tau_{av}$ are the production rates of the primary runaway electrons (Dreicer acceleration) [6,7] and secondary knock-on avalanche [17], accordingly, and τ_{loss} represents the time constant of the runaway losses. The Dreicer acceleration rate is a function of $\epsilon = E/E_c$:

$\tau_{dr}^{-1} \approx 0.3\nu_e \epsilon^{-3(Z_{\rm eff}+1)/16} \exp[-1/(4\epsilon) - \sqrt{(Z_{\rm eff}+1)/\epsilon}\,]$, where E_c is the critical electric field given by $E_c = e^3 n_e Z_{\rm eff} \ln\Lambda/(4\pi\epsilon_0^2 m_e v_{\rm th}^2)$, ν_e is the collision frequency of the electrons at the thermal velocity $v_{\rm th}$, and $Z_{\rm eff}$ is the effective plasma charge. The time constant of the knock-on avalanche is described by the relation $\tau_{av} \approx 2m_e c \ln\Lambda a(Z_{\rm eff})/(eE)$, where $a(Z_{\rm eff} = 1) \approx 1$ [11,17]. Macroscale magnetic turbulence can constitute the dominant losses of runaway electrons during the disruption [11,18]. The time constant $\tau_{\rm loss}$ can be described in this case by the relation: $\tau_{\rm loss} \approx k_t(\delta B/B_t)^{-2}$, where $k_t \approx \delta r_t^2/(\pi R_0 q v_r)$, δr_t—the radial extension of the turbulent area and magnetic field perturbations are considered as radial functions decaying outside the resonant magnetic surface.

Calculations of the runaway production rate depend critically on the amplitude of the electric field generated during reconnection. Detailed calculations of the field require 3D MHD simulations (see [16]), which are complicated in real experimental conditions. In a simplified way, the longitudinal electric field induced during the sawtooth crash around the $q = 1$ surface can be estimated using measured radial velocity of the plasma core ($m = 1$ displacement rate). Generation of the electric field up to $E \sim 10$ V/m for time duration of $t_{\rm crash} \sim 0.1$ ms can be predicted in this case. Similar values of the electric field can be obtained from the calculation of the inductive response to the reduction of poloidal magnetic flux during the sawtooth crash. A schematic view of the process is shown in Fig. 4a. The growth of the MHD ($m = 1$) mode leads to generation of the electric field around the resonant ($q = 1$) surface. An induced electric field provides acceleration of the electrons which is accompanied by bursts of nonthermal x-ray emission. Calculations (see Figs. 4b and 4c) indicate that electric field $E \approx 10$ V/m can induce a runaway beam with density $N_r \approx 7 \times 10^{17}$ m^{-3} in a narrow region ($\delta r/r_s \approx 0.1$) around the resonant surface. Magnetic turbulence ($k_t \approx 6 \times 10^{-12}$ s) generated during sawtooth relaxation leads to outward displacement of the runaway beam (see Fig. 4d). The calculated growth rate ($\gamma_r \sim 10^4$ s^{-1}) and velocity of the electron beam propagation outside the $q = 1$ surface ($V \sim 10^3$ m/s) agrees with the ones determined from the analysis of x-ray perturbations observed in the experiments (see Fig. 4e).

The simple model described in the paper allows phenomenological description of runaway production, while simulations using kinetic and MHD codes are ultimately required for detailed analysis of the process. Nevertheless, analysis of the experiments indicates that suprathermal electrons can play an important role during reconnection and should be considered in analysis of the disruption phenomena and in interpretation of the experimental measurements in tokamaks. In particular, generation of nonthermal electrons can possibly explain the abrupt trigger and short time scale of the internal reconnection as well as fast (ballistic) heat pulse propagation at the outer radii. Moreover, in spite of the fact that the total number of suprathermal electrons during the crash is small, they can induce runaway current comparable with one inside the $q = 1$ surface (I_r is of the order of 20 kA). Growth of runaway current during the internal reconnection (sawtooth crash) veils decay of the equilibrium plasma current, which can explain in part small changes of the $q(r)$ profile observed in experiments on tokamaks with the use of Faraday rotation and motional Stark effect diagnostics (see references in [2,9]).

The author would like to thank S. Von Goeler, S. V. Mirnov, F. M. Stefanovskij, and R. J. Hastie for stimulating discussions, and A. V. Khramenkov, I. V. Klimanov, A. V. Sushkov, and V. M. Trukhin for help with the experiments. This work was supported by RFBR Grant No. 98-02-17382.

[1] B. B. Kadomtsev, *Tokamak Plasma: A Complex Physical System* (IOP Publishing Ltd., Bristol, 1992).
[2] D. Biskamp, *Nonlinear Magnetohydrodynamic* (Cambridge University Press, Cambridge, England, 1993).
[3] M. Yamada *et al.,* Phys. Plasmas **1**, 3269 (1994).
[4] E. R. Priest, *Solar Magnetohydrodynamic* (Reidel, Dordrecht, 1984).
[5] S. Masuda, Nature (London) **371**, 495 (1994).
[6] H. Dreicer, Phys. Rev. **117**, 329 (1960).
[7] V. V. Parail and O. P. Pogutse, *Reviews of Plasma Physics* (Consultants Bureau, New York, 1986), Vol. 11, pp. 1–68.
[8] S. Von Goeler, W. Stodiek, and N. Sauthoff, Phys. Rev. Lett. **33**, 1201 (1974).
[9] F. C. Schuller, Plasma Phys. Controlled Fusion **37**, A135 (1995).
[10] R. D. Gill *et al.,* Nucl. Fusion **40**, 163 (2000).
[11] R. Yoshino and S. Tokuda, Nucl. Fusion **40**, 1293 (2000).
[12] R. Jaspers *et al.,* Phys. Rev. Lett. **72**, 4093 (1994).
[13] P. V. Savrukhin *et al.,* Rev. Sci. Instrum. **70**, 591 (1999).
[14] P. V. Savrukhin *et al.,* Nucl. Fusion **34**, 317 (1994).
[15] G. Taylor *et al.,* Nucl. Fusion **32**, 1867 (1992).
[16] W. Park, D. A. Monticello, E. D. Fredrickson, and K. McGuire, Phys. Fluids B **3**, 507 (1991).
[17] M. N. Rosenbluth and S. V. Putvinski, Nucl. Fusion **37**, 1355 (1997).
[18] A. B. Rechester and M. N. Rosenbluth, Phys. Rev. Lett. **40**, 38 (1978).